First-principles study on the electronic, optical, and transport properties of monolayer α- and β-GeSe

Yuanfeng Xu, Hao Zhang, Hezhu Shao, Gang Ni, Jing Li, Hongliang Lu, Rongjun Zhang, Bo Peng, Yongyuan Zhu, Heyuan Zhu, and Costas M. Soukoulis

Phys. Rev. B **96**, 245421 — Published 22 December 2017

DOI: 10.1103/PhysRevB.96.245421

First-principle study on the electronic, optical and transport properties of monolayer α and $\beta-$GeSe

Yuanfeng Xu[1], Hao Zhang[1,4,5†], Hezhu Shao[2], Gang Ni[1], Jing Li[1], Hongliang Lu[3], Rongjun Zhang[1], Bo Peng[1], Yongyuan Zhu[4], Heyuan Zhu[1,‡] and Costas M. Soukoulis[5,6]

[1]*Department of Optical Science and Engineering and Key Laboratory of Micro and Nano Photonic Structures (Ministry of Education), Fudan University, Shanghai 200433, China.*

[2]*Ningbo Institute of Materials Technology and Engineering, Chinese Academy of Sciences, Ningbo 315201, China*

[3]*State Key Laboratory of ASIC and System, Institute of Advanced Nanodevices, School of Microelectronics, Fudan University, Shanghai 200433, China*

[4]*National Laboratory of Solid State Microstructure, Nanjing University, Nanjing 210093, China*

[5]*Department of Physics and Astronomy and Ames Laboratory, Iowa State University, Ames, Iowa 50011, USA*

[6]*Institute of Electronic Structure and Laser (IESL), FORTH, 71110 Heraklion, Crete, Greece*[*]

(Dated: December 4, 2017)

The extraordinary properties and the novel applications of black phosphorene induce the research interest on the monolayer group-IV monochalcogenides. Here using the first-principles calculations, we systematically investigate the electronic, transport and optical properties of monolayer $\alpha-$ and $\beta-$GeSe, revealing a direct of 1.61 eV of monolayer $\alpha-$GeSe and an indirect band gap of 2.47 eV of monolayer $\beta-$GeSe. For monolayer $\beta-$GeSe, the electronic/hole transport is anisotropic with an extremely high electron mobility of $2.93 \times 10^4 cm^2/V \cdot s$ along the armchair direction, and comparable to that of black phosphorene. Furthermore, for $\beta-$GeSe, robust band gaps nearly disregarding the applied tensile strain along the armchair direction is observed. Both monolayer $\alpha-$ and $\beta-$GeSe exhibit anisotropic optical absorption in the visible spectrum.

I. INTRODUCTION

The atomic-monolayer materials, also called as two-dimensional (2D) materials, have received tremendous attentions since the experimental realization of graphene[1–3]. Nowadays, 2D materials have formed a large material family, involving various kinds of layered crystal structures and chemical elements, e.g. graphene[4–6], transition metal dichalcogenides (TMDs)[7–10], stanene[11, 12], penta-graphene[13, 14], and etc.

Recently, black phosphorene, a monolayer material composed of phosphorus atoms with puckered structure, attracts much attention for its extraordinary properties. Black phosphorene is a semiconductor with a direct band gap of 1.5 eV [15, 16], and it has strongly anisotropic transport property with a high hole mobility comparable to graphene [16–19], which make it a promising candidate for future electronic and optoeletronic applications. Many efforts have been devoted on the discovery of new 2D materials with "phosphorene analogues" puckered structure[20], since the successful prediction of black phosphorene. Followed by the prediction approach proposed as the "atomic transmutation" method[21], that one type of elements is changed (transmutationed) into its neighboring elements in the periodic table but the total number of valence electrons is kept unchanged, the monolayer of group-IV monochalcogenides MX (M=Ge, Sn; X=S, Se) with similar puckered structures is believed to possess similar properties with black phosphorene, and can be regarded as a family of "phosphorene analogues"[20, 22–24].

The properties of the material family MX in the bulk form have been intensely investigated and revealed to be excellent thermoelectric materials with high figure of merit[25], especially for the crystal SnSe with an extraordinarily high thermoelectric ZT value of 2.6 ± 0.3 at 923K[26]. Much attention has been devoted on studying electronic and optical properties[20, 22], piezoelectricity[23, 24], thermoelectric and phonon transport[25] properties of monolayer MX. Recently Rohr *et al.* predicted a new member of MX family, *i.e.* $\beta-$GeSe, which is a polymorph of GeSe[27] with a boat conformation for its Ge-Se six-membered ring. Experimental measurement and theoretical calculations reveal that monolayer $\beta-$GeSe, similar to another polymorph of GeSe, *i.e.* $\alpha-$GeSe[28], is a semiconductor with a moderate band gap as well, which make it promising for future electronic and optoelectronic applications. Further investigations on monolayer $\beta-$GeSe and some related monolayer MX crystals are thus necessary to gain insights on this new kind of 2D materials.

In this work, we systematically investigate the electronic, transport and optical properties of monolayer $\alpha-$ and $\beta-$GeSe by using first-principles calculations. We demonstrate that the direct band gap of monolayer $\alpha-$GeSe is smaller than the indirect band gap of $\beta-$GeSe. Both monolayers of $\alpha-$ and $\beta-$ GeSe have exceptionally high electron mobility, which are predicted to be 4.71 $\times 10^3 cm^2/V \cdot s$ and $2.93 \times 10^4 cm^2/V \cdot s$ respectively with strong anisotropy. Furthermore, we also investigate the strain-engineering and optical properties of these two ma-

[*] [†]zhangh@fudan.edu.cn; [‡]hyzhu@fudan.edu.cn

terials.

II. METHOD AND COMPUTATIONAL DETAILS

The calculations are performed using the Vienna *ab-initio* simulation package (VASP) based on density functional theory[29]. The exchange-correlation energy is described by the generalized gradient approximation (GGA) using the Perdew-Burke-Ernzerhof (PBE) functional. The calculation is carried out by using the projector-augmented-wave (PAW) pseudopotential method with a plane wave basis set with a kinetic energy cutoff of 600 eV. Furthermore, for Ge and Se atoms, we considered d and p semicore states respectively as valence states by choosing Ge_d and Se pseudopotentials. When optimizing atomic positions, the energy convergence value between two consecutive steps is chosen as 10^{-5} eV and the maximum Hellmann-Feynman force acting on each atom is 10^{-3} eV/Å. For $\alpha-$GeSe monolayer, the Monkhorst-Pack scheme is used for the Brillouin zone integration with k-point meshes of 17×15×1 and 25×21×1 for geometry optimization and self-consistent electronic structure calculations, respectively. And for β phase, we use 17×11×1 and 25×15×1 Monkhorst-Pack k meshes for the structure relaxation and electronic structure calculations, respectively. To verify the results of the PBE calculations, the electronic structures of $\alpha-$ and $\beta-$GeSe are calculated using the much more computationally expensive hybrid Heyd-Scuseria-Ernzerhof (HSE06) functional[30, 31]. Generally, HSE06 improves the precision of band gap by reducing the localization and delocalization errors of PBE and HF functionals. Hereby, the screening parameter u is set to 0.2 $Å^{-1}$. The complex dielectric functions $\epsilon(\omega)$ of monolayer $\alpha-$ and $\beta-$GeSe are calculated by using HSE06 hybrid functional on a grid of 11×11×1. The tetrahedron method with Blöchl corrections is used as the smearing scheme. The effect of the van der Waals (vdW) interactions between adjacent layers was considered by using the empirical correction scheme of the Grimme's DFT-D2 (PBE-D2) method[32, 33].

The properties of monolayer $\alpha-$ and $\beta-$GeSe are obtained based on the results of complex dielectric function, *i.e.* $\epsilon(\omega) = \epsilon_1(\omega) + i\epsilon_2(\omega)$. The imaginary part of dielectric tensor $\epsilon_2(\omega)$ is determined by a summation over empty band states as follows [34],

$$\epsilon_2(\omega) = \frac{2\pi e^2}{\Omega\epsilon_0} \sum_{k,v,c} \delta(E_k^c - E_k^v - \hbar\omega) \left| \langle \Psi_k^c | \mathbf{u}\cdot\mathbf{r} | \Psi_k^v \rangle \right|^2, \quad (1)$$

where ϵ_0 is the vacuum dielectric constant, Ω is the crystal volume, v and c represent the valence and conduction bands respectively, $\hbar\omega$ is the energy of the incident photon, $\mathbf{u}$ is the vector defining the polarization of the incident electric field, $\mathbf{u}\cdot\mathbf{r}$ is the momentum operator, Ψ_k^c and Ψ_k^v are the wave functions of the conduction and valence band at the k point, respectively. The real part of dielectric tensor $\epsilon_1(\omega)$ is obtained by the well-known Kramers-Kronig relation[35],

$$\epsilon_1(\omega) = 1 + \frac{2}{\pi} P \int_0^\infty \frac{\epsilon_2(\omega')\omega'}{\omega'^2 - \omega^2 + i\eta} d\omega', \quad (2)$$

where P denotes the principle value. The absorption coefficient $\alpha(\omega)$ and reflectivity $R(\omega)$ can be subsequently given by [36–38]

$$\alpha(\omega) = \frac{\sqrt{2}\omega}{c} \left\{ \left[\epsilon_1^2(\omega) + \epsilon_2^2(\omega)\right]^{1/2} - \epsilon_1(\omega) \right\}^{\frac{1}{2}}, \quad (3)$$

$$R(\omega) = \left| \frac{\sqrt{\epsilon_1(\omega) + i\epsilon_2(\omega)} - 1}{\sqrt{\epsilon_1(\omega) + i\epsilon_2(\omega)} + 1} \right|^2, \quad (4)$$

By using the deformation potential theory for semiconductors, which was proposed by Bardeen and Shockley[39], the intrinsic carrier mobility μ of monolayer group-IV monochalcogenides: $\alpha-$GeS, $\alpha-$GeSe, $\alpha-$SnS, $\alpha-$SnSe, and $\beta-$GeSe is calculated and investigated in details herein. In the long-wavelength limit, when only considering the interaction between electron and longitudinal acoustic phonon[39, 40], the carrier mobility of 2D semiconductors is given by [41–44],

$$\mu = \frac{e\hbar^3 C^{2D}}{k_B T m_e^* m_d E_l^2}, \quad (5)$$

where e is the electron charge, $\hbar$ is the reduced Planck's constant, T is the temperature equal to 300 K throughout the paper. C^{2D} is the elastic modulus of a uniformly deformed crystal by strains and derived from $C^{2D} = [\partial^2 E/\partial^2(\Delta l/l_0)]/S_0$, in which E is the total energy, Δl is the change of lattice constant l_0 along the transport direction, and S_0 represents the lattice volume at equilibrium for a 2D system, m_e^* is the effective mass along the transport direction given by $m_e^* = \hbar^2(\partial^2 E(k)/\partial k^2)^{-1}$ (k is wave-vector, and $E(k)$ denotes the energy) (either m_a^* or m_b^* along the a or b direction, respectively), m_d is the average effective mass defined by $m_d = \sqrt{m_a^* m_b^*}$. E_l is the deformation potential (DP) constant defined by $E_l^{e(h)} = \Delta E_{CBM(VBM)}/(\Delta l/l_0)$, where $\Delta E_{CBM(VBM)}$ is the energy shift of the band edge with respect to the vacuum level under a small dilation Δl of the lattice constant l_0.

III. RESULTS AND DISCUSSION

A. Geometric structure of monolayer $\alpha-$ and $\beta-$GeSe

The top and side view of the fully optimized structure of monolayer $\alpha-$ and $\beta-$GeSe both with space group of

TABLE I. Structural informations, cohesive energies (E_c), SOC strength (E^{SOC}) and band gaps of monolayer $\alpha-$ and $\beta-$GeSe. The bond angles of θ and bond lengths of d are indicated in Fig. 1.

phase	a	b	d_1	d_2[Å]	θ_1	θ_2[°]	$E_c[eV/atom]$	E^{SOC}_{Ge}	$E^{SOC}_{Se}[eV]$	$E_g(PBE(SOC)/HSE06(SOC))[eV]$
α	3.97(3.83[27])	4.29(4.39[27])	2.54	2.66	96.59	97.41	-4.20	-0.016	-0.040	1.16(0.18)/1.61(1.67)
β	3.67(3.83[27])	5.91(5.81[27])	2.55	2.72	96.65	93.91	-4.17	-0.016	-0.041	1.76(0.80)/2.47(2.53)

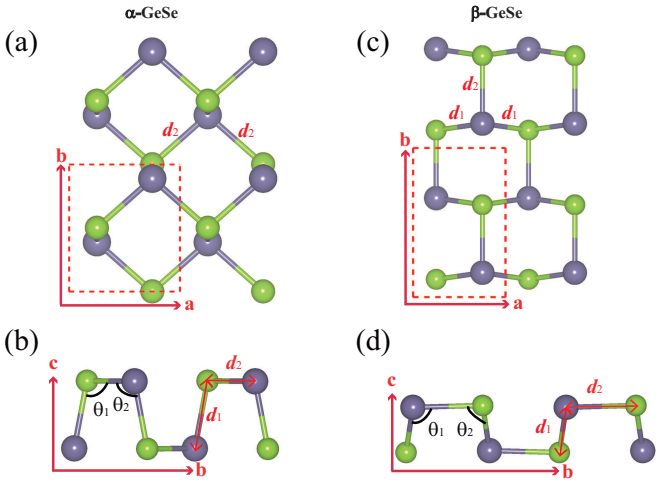

FIG. 1. Atomic structure of monolayer $\alpha-$ and $\beta-$GeSe in a 2×2×1 supercell from top view (a,c) and side view (b,d), respectively. The a/b direction is the zigzag/armchair direction, respectively. The blue and green balls denote Ge and Se atoms respectively.

$Pmn2_1(31)$ are shown in Fig. 1 ((a), (b)) and ((c), (d)), respectively. Both monolayer $\alpha-$ and $\beta-$GeSe consist of two atomic sublayers. The $\alpha-$ and $\beta-$GeSe monolayer are optimized with vacuum layers of 21 $\AA$ and 16$\AA$, respectively, which are large enough to avoid the artificial interaction between atom layers. The tetragonal unit cell (the dashed rectangle) of monolayer $\alpha-$ and $\beta-$GeSe contains two germanium atoms and two selenium atoms. From the top view and side view of $\alpha-$GeSe as shown in Fig. 1 (a) and (b), monolayer $\alpha-$GeSe is a puckered structure analogue to black phosphorene with Ge and Se atoms substituted for P atoms alternately[15, 45, 46]. Similar monolayer structures can be found in monolayer black phosphorene and other group-IV monochalcogenides MX (M=Ge or Sn; X=S or Se), e.g., $\alpha-$GeS, $\alpha-$GeSe, $\alpha-$SnS and $\alpha-$SnSe, as shown in the Supplemental Material[47].

Monolayer $\beta-$GeSe, which consists of six-rings with the vertices arranged in an uncommon boat conformation[27] as shown in Fig. 1 (c,d), can be mechanically exfoliated from the bulk phase due to the weak van der Waals bonding between adjacent monolayers, and Supplemental Material[47] shows the structures of bulk and monolayer $\beta-$GeSe from the top and side view.

Based on the first-principles method, the lattice constants of $\alpha-$GeSe are calculated to be $a = 3.97$ $\AA$ and $b = 4.29$ $\AA$, which are in good accordance with reported experimental ($a = 3.83$ $\AA$ and $b = 4.39$ $\AA$)[27] and theoretical ($a = 3.96$ $\AA$ and $b = 4.16$ $\AA$ in Ref. [48], $a = 3.93$ $\AA$ and $b = 4.27$ $\AA$ in Ref. [24] and $a = 3.90$ $\AA$ and $b = 4.24$ $\AA$ in Ref. [49]) results. Each Ge/Se atom binds three neighboring Se/Ge atoms with different bond lengths, as shown in Fig.1 (a,b), and two of them are identical with $d_2 = 2.66$ $\AA$ and the other one is $d_1 = 2.54$ $\AA$. The bond angles of $\theta_{Ge-Se-Ge}$ and $\theta_{Se-Ge-Se}$ are 96.59° and 97.41°, respectively. For monolayer $\beta-$GeSe, the optimized lattice constants are $a = 3.67$ $\AA$ and $b = 5.91$ $\AA$, which are in good agreement with experimental results ($a = 3.83$ $\AA$ and $b = 5.81$ $\AA$)[27]. In this boat structure of $\beta-$GeSe, each Ge atom binds three Se atoms with two identical bond lengths of $d_1 = 2.55$ $\AA$ and one bond length of $d_2 = 2.72$ $\AA$, and the bond angles of $\theta_{Ge-Se-Ge}$ and $\theta_{Se-Ge-Se}$ are 93.91° and 96.65°, respectively. For comparison, the calculated lattice parameters, bond lengths, and bond angles for black phosphorene and other $\alpha-$structure of group-IV monochalcogenides MX are shown in Table. S1.

For monolayer $\alpha-$GeSe shown in Fig. 2 (a), both the conduction band minimum (CBM) and the valence band maximum (VBM) are located along the $\Gamma - Y$ direction denoted by C_y and V_y respectively. The formation of the band gap of $\alpha-$GeSe shows that it is a semiconductor with a direct band gap of 1.16 eV, which is well consistent with the reported results (1.16 eV in Ref. [25] and Ref. [47], 1.22 eV in Ref. [49])[25, 48, 50]. However, it is worthy to mention that the energy difference (0.014 eV) between the local CBMs (C_X and C_Y in Fig. 2 (a)) and the CBM at k_{CBM} is very small, and such nearly degenerate CBMs suggest that it is feasible to apply some kinds of external controls (e.g. strain), to tune monolayer $\alpha-$GeSe from direct to indirect semiconductors, or vice versa. Since Ge and Se are relatively heavy elements, the SOC effect may influence the band structures obviously, which is confirmed by the calculated band structures with SOC involved, as shown in Fig. 2 (a) (the red dashed line). The corresponding HSE06 calculation without SOC (with SOC) in Fig. 2 (b) (Fig. 2 (c)) gives a larger band gap of 1.61 eV (1.67 eV) compared to the PBE result of 1.16 eV, since PBE calculations always underestimate the value of band gaps of semiconductors.

As mentioned above, the $\alpha-$structure of group-IV monochalcogenides MX can be regarded as the results of material design by "atomic transmutation" from monolayer black phosphorene, in which the P atoms are changed by group-IV atom (Ge/Sn) and group-VI atom (S/Se) and the total number of valence electrons is kept unchanged. Therefore the similarity of electronic band

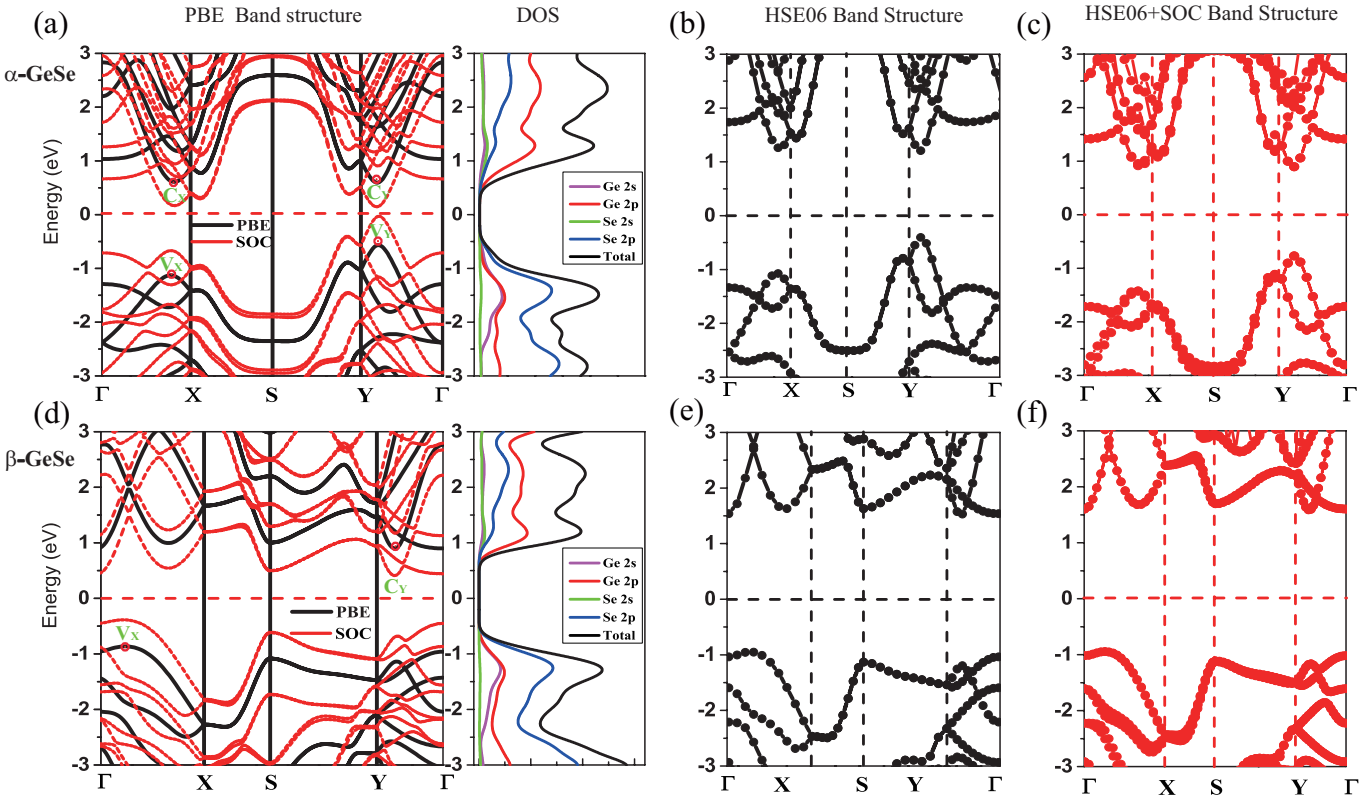

FIG. 2. (a) and (d) are PBE calculations with and without SOC of electronic band structure and PBE calculated density of states (DOS) of monolayer $\alpha-$GeSe and $\beta-$GeSe along high-symmetry directions respectively. (b) and (e) are the electronic band structures under HSE06 hybrid functional of monolayer $\alpha-$GeSe and $\beta-$GeSe respectively, and (c) and (f) are the HSE06 band calculations with SOC.

structures between monolayer black phosphorene and $\alpha-$MX is expected (results shown in the Supplemental Material[47]), resulting from the structural similarity and the similar p-orbital electrons contributions. By comparison with the band gaps of black phosphorene and other monolayer $\alpha-$MX under investigations here (Supplemental Material[47]) it is found that only black phosphorene and $\alpha-$GeSe possess direct band gaps, while the other "phosphorene analogues" including $\beta-$GeSe possess indirect band gaps, which means that only monolayer black phosphorene and $\alpha-$GeSe possess good ability to absorb photons, while the photon-absorption abilities of $\beta-$GeSe and other $\alpha-$MX are relatively poor since photons are necessarily involved.

The PBE calculations with and without SOC for the electronic band structure and DOS of monolayer $\beta-$GeSe are presented in Fig. 2 (d), which shows that, monolayer $\beta-$GeSe is a semiconductor with an indirect band gap with $E_g = 1.76$ eV. The CBM locates at the midpoint along $\Gamma - Y$ direction and the VBM locates near the Γ point along the $\Gamma - X$ direction. The obtained band gap decreases to 0.80 eV when the SOC is involved. The HSE06 calculations with and without SOC effects for $\beta-$GeSe give the band gap of 2.53 eV and 2.47 eV, respectively, which are larger than that of $\alpha-$GeSe.

As for the SOC effects, since the calculated SOC strength is negative as shown in Table. I, the calculated band gaps for both $\alpha-$ and $\beta-$GeSe decrease when SOC is involved.

In order to clarify the contributions from different orbitals to the band structures around the Fermi level of $\alpha-$ and $\beta-$GeSe, we calculate the total and partial density of states (DOS) as shown in the right part of Fig. 2 (a) and (e). Analysis on the PDOS (Ge-4s, 4p and Se-4s, 4p orbitals) of $\alpha-$GeSe reveals that Ge-4p and Se-4p orbitals dominate the electronic states near the Fermi level. The contributions from the Ge-4p to the total DOS of the conduction bands is larger than that from Se-4p, while in the valence band, the Se-4p orbitals have more contributions than those from Ge-4p. Analysis on the PDOS of monolayer $\beta-$GeSe reveals the dominant contributions from Ge-4p and Se-4p orbitals to the total DOS near the Fermi level, and the respective contribution from the Ge-4p and Se-4p orbitals is similar to the case of $\alpha-$GeSe. Similar analysis of PDOS on other $\alpha-$MX also leads to the result that the p orbital of group-IV (group-VI) atoms dominates the conduction (valence) bands. It is worthy to note that, to correct the underestimation of the bandgap of standard DFT calculations, the DFT+U approach can be used by setting the on-site Coulomb parameter U and J to Ge atoms.

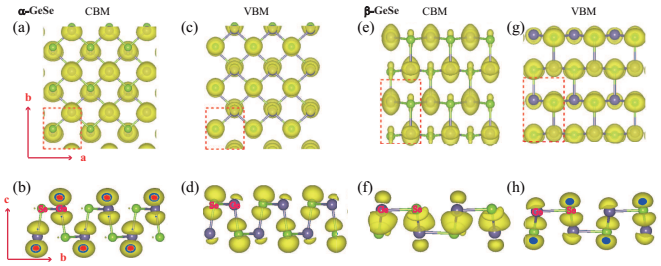

FIG. 3. Iso-surface plots of the charge density of CBM ((a, b)), VBM ((c, d)) for monolayer $\alpha-$GeSe and CBM ((e, f)), VBM ((g, h)) for monolayer $\beta-$GeSe illustrated in the ab and bc plane, with an iso-value of of 0.007 $e/\AA^3$.

B. Electronic band structure of 2D $\alpha-$ and $\beta-$GeSe

The calculated electronic band structures performed by both PBE (with and without spin-orbital-coupling, SOC) and HSE06-hybrid functional method for monolayer $\alpha-$ and $\beta-$GeSe along high-symmetry directions of Brillouin zone (BZ) are shown in Fig. 2. The above-mentioned PDOS analysis on the orbitals contributions to the formation of CBM and VBM is validated by the partial charge densities associated with the CBM and VBM both for monolayer $\alpha-$ and $\beta-$GeSe, as shown in Fig. 3. In both materials, the p orbitals of Ge atoms contributes dominantly to CBM by connecting the neighboring Se atoms via antibonding states, as shown in Fig. 3 (a-b) and (e-f), however, VBM is dominated by the contribution from p orbitals of Se atoms by connecting the neighboring Ge atoms via bonding states, as shown in Fig. 3 (c-d) and (g-h).

C. Strain-engineering electronic properties of monolayer $\alpha-$ and $\beta-$GeSe

Here, we study the effects of in-plane uniaxial (a and b direction) and biaxial (bi: **a** + **b** direction) strains on electronic properties of monolayer $\alpha-$ and $\beta-$GeSe, to realize the possible tunability of their electronic properties[51]. In this work, ε_x, ε_y and ε_{xy} indicate the components of the relative strain along a, b and bi directions respectively. The positive (negative) values represent tensile (compressive) strain, and evaluated as the lattice stretching (condensing) percentage. All the applied strains here are in the elastic region[52], which is confirmed by the quadratic dependence of strained energy on the applied strains (in Supplemental Material[47]).

Fig. 4 shows the valence and conduction band structures of monolayer $\alpha-$GeSe as a function of different strains, from -10% to 10% of the fully relaxed structure. Fig. 4 (a-c) show the dependence of the energy bands on strain along a, b and bi direction, respectively. Fig. 4 (d) shows the evolution of calculated band gap under various strains.

The VBMs (V_X and V_Y) and CBMs (C_X and C_Y) are shown in Fig. 4. Monolayer $\alpha-$GeSe without strains is a direct semiconductor described by VBM of V_Y and CBM of C_Y. When compressive strains are applied along a direction, the values of V_Y and C_Y increase, while the value of C_X decreases, leading to a transition from direct to indirect semiconductor of monolayer $\alpha-$GeSe even at a small compression with ε_x=-1%. When a compressive strain of ε_x=-8% is applied, a semiconductor-to-metal transition takes place as shown in Fig. 4 (d).

However, when applying a tensile strain along a direction, the changes of the local VBM and CBM are different. When the tensile strain increases, the value of local V_Y decreases, and the values of C_X and V_X increase, while the value of C_Y keeps nearly unchanged, subsequently leading to a transition from direct to indirect semiconductors at ε_x=9%. So, the direct band gap characteristic of monolayer $\alpha-$GeSe keeps unchanged for small compression and moderate stretching along a direction (from ε_x=-1% to ε_x=9%).

The change of the band structures of monolayer $\alpha-$GeSe when applying an external strain along b direction (ε_y) is much smaller than that for strains along a direction, similar analysis on the evolution of band structures for compressive and tensile strains, as shown in Figs. 4 (b) and (d), show that, for applied strains from -10% to 10%, a transition from direct to indirect semiconductor happens, while the transition from semiconductor to metal does not takes place in the strain region.

When applying strains along the bi direction from -10% to 10%, the changes of the band structures are more similar to those for strains along the a direction, and the transitions for both direct-to-indirect semiconductor and semiconductor-to-metal happen, as shown in Figs. 4 (c) and (d), except that the latter transition occurs at a compressive strain of ε_{xy}=-6%.

In addition, the evolution of band gaps in $\alpha-$GeSe under various strains are shown in Fig. 4 (d), indicating that the values of the calculated band gaps increase with the increase of tensile strains in the region from -10% to 10%, disregarding the directions along which the the strains were applied.

Fig. 5 shows the evolutions of band structures and values of band gap of monolayer $\beta-$GeSe as a function of compressive and tensile strains with the strength from -10% to 10%. The behavior of $\beta-$GeSe under strains is quite different compared to that of $\alpha-$GeSe. Monolayer $\beta-$GeSe without strain is an indirect semiconductor described by VBM of V_X and CBM of C_Y. When compressive strains are applied along a direction, the values of V_X, C_X and C_Y decrease, while V_S increase, leading to another type of indirect semiconductor. When applying a tensile strain along a direction, the change of these VBMs and CBMs are on the contrary tendencies compared to that of compressive strain. We compared the evolutions of band structures under strain along b and bi directions as shown in Fig. 5 (b) and (c), and came to the conclusion that the tendency of V_X, C_X and C_Y are simi-

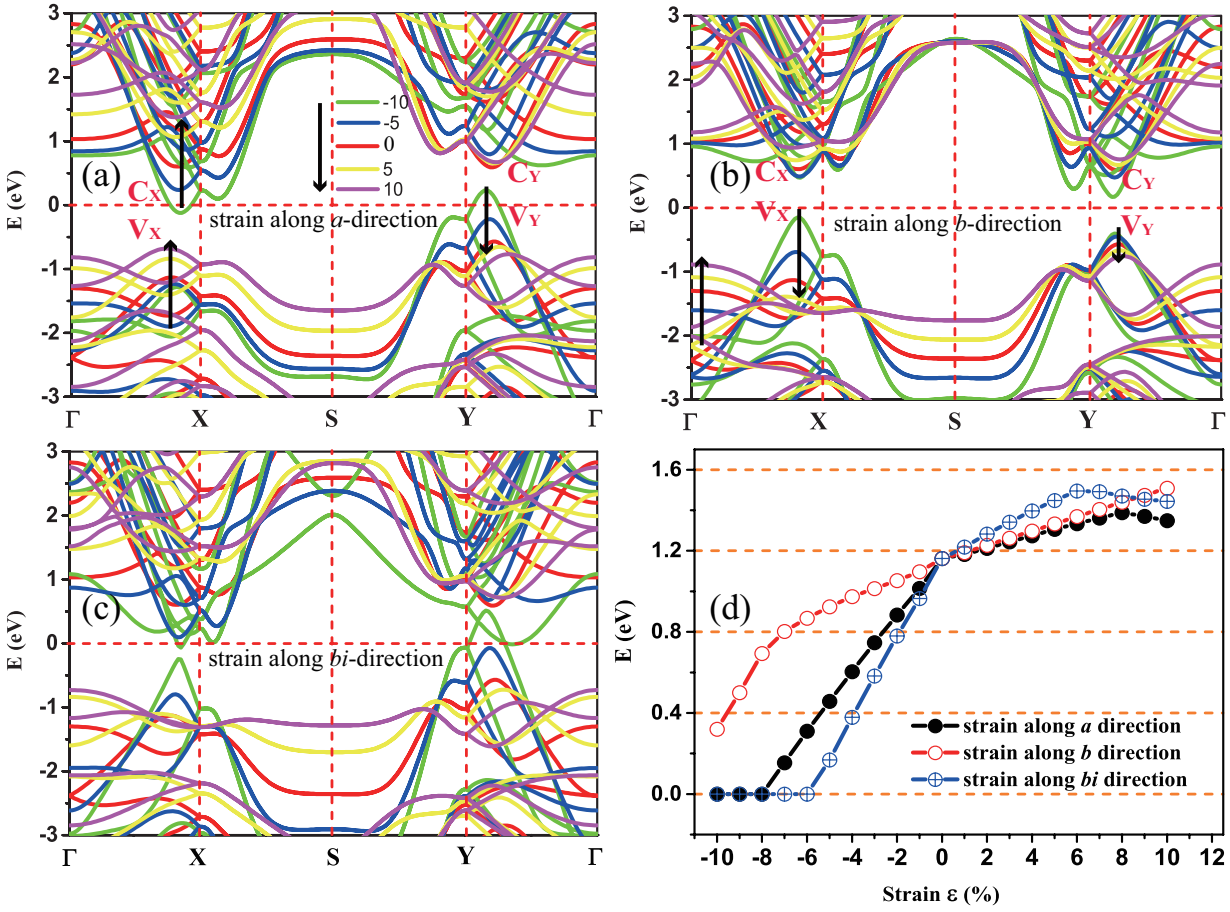

FIG. 4. Electronic band structures of monolayer $\alpha-$GeSe under applied strains along (a) a direction,(b) b direction and (c) bi direction. (d) shows the evolution of band gaps for $\alpha-$GeSe as a function of the applied strain.

lar with that of along a direction, but with large changes of V_S in the strain range from -10% to 10%. Furthermore, there is no transition from semiconductor to metal in this strain region.

It should be noted here that, although the band gap of monolayer $\beta-$GeSe decreases when the applied compressive strains increase, which is similar to the case of $\alpha-$GeSe, however, the decreasing tendency of band gap when increasing tensile strains is opposite to that of $\alpha-$GeSe. More interestingly, as shown in Fig. 5 (b,d), for applied tensile strains along b direction from 0% to 10%, both VBM (V_x) and CBM (C_x) locate along $\Gamma - X$ direction and the values of VBM and CBM keep nearly unchanged, which means that the calculated band gaps subsequently keep nearly unchanged, around 1.73 eV. Such robust band gap nearly disregarding the tensile strains also leads to the nearly overlap of bandgap curves for the two respective cases by applying tensile strains along a and bi directions, as shown in Fig. 5(d).

As we know that band gap is related to the bonding-antibonding splitting, which is determined quantitively by the overlap integral V of atomic orbitals. The overlap integral V decreases with increasing the interatomic distance, following the d^{-2} principle (d is the bond length) in covalent solids[53], *i.e.* $V \propto d^{-2}$. Thus, the energy width of each band increases when compressive strains are applied, since the corresponding value of V increases due to a smaller of d, as shown in Fig. 4 (a,b) and Fig. 5 (a,b). Similarily, when the tensile strains are applied, the band structure for covalent solids tends to be flat gradually, due to the smaller value of V caused by a larger d. As shown in Table. 1 and Fig. 1 (d), monolayer $\beta-$GeSe has a relatively large bond length (d_2) along b direction. It means that the overlap integral along b direction is smaller than that along a direction, indicating that the change of band gap when applying tensile strains along b direction will be much weaker.

To further understand the bond characteristics and then the mechanism of the robust band gap for monolayer $\beta-$GeSe, we have calculated the electronic localization function (ELF)[54–57] as shown in Fig. 6. ELF is a position dependent function with values that range from 0 to 1. ELF = 1 corresponds to perfect localization and ELF = 0.5 corresponds to the electron-gas like pair probability. 3D plot of the ELF in Fig. 6 (a) shows that the covalent bond strength along b direction is trivial compared with that along a direction, which is reflected as well by the charge densities distribution for VBM and

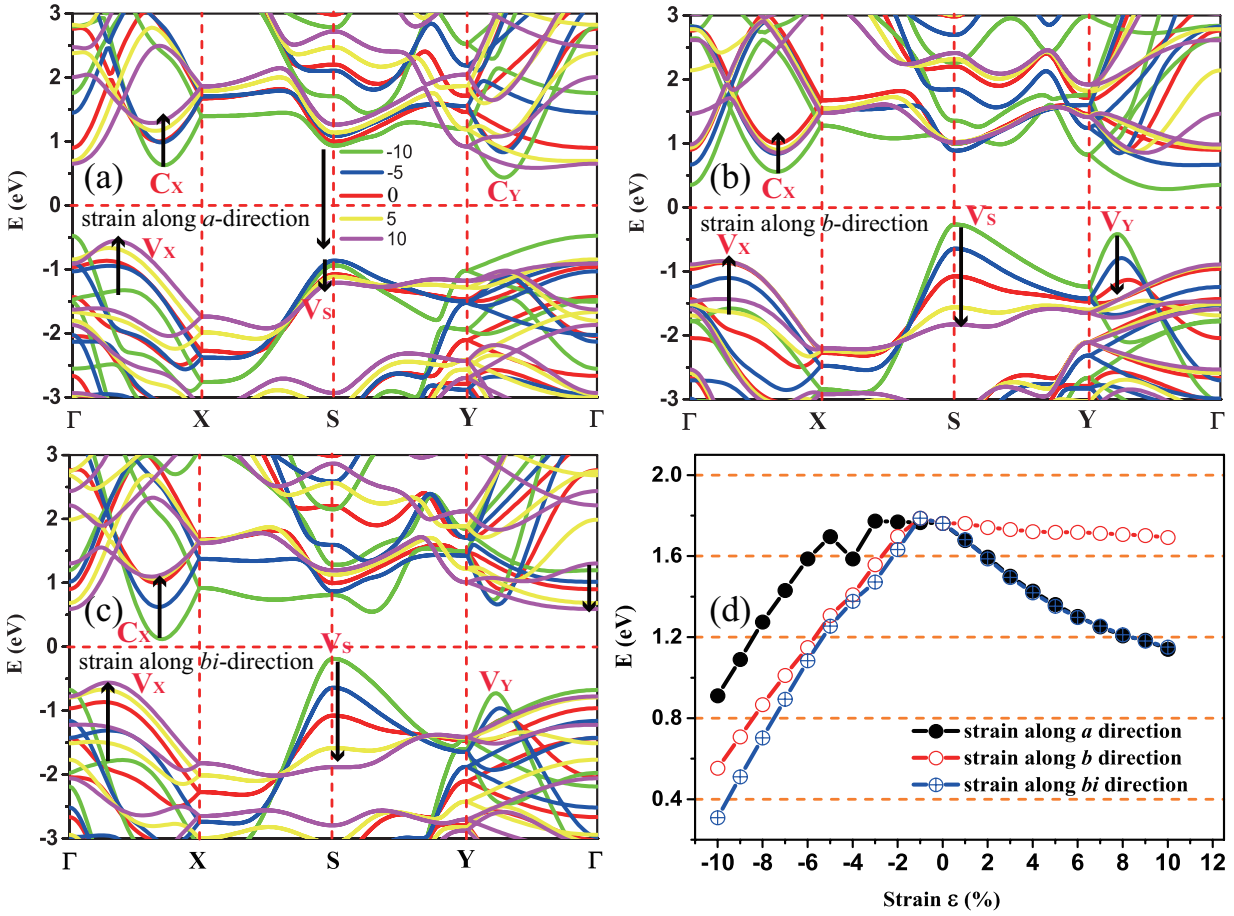

FIG. 5. Electronic band structures of monolayer $\beta-$GeSe under applied strains along (a) a direction,(b) b direction and (c) bi direction. (d) shows the evolution of band gaps for $\beta-$GeSe as a function of the applied strain.

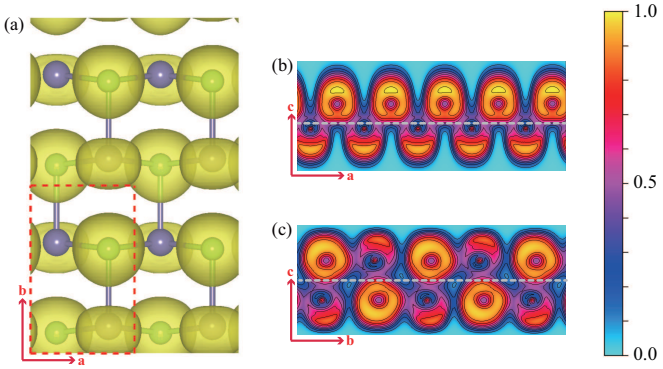

FIG. 6. (a) Top view of 3D ELF and 2D ELF profiles of monolayer $\beta-$GeSe along the (b) a and (c) b direction, respectively.

CBM shown in Fig. 3. 2D plots of ELF profiles in Fig. 6 (b) and (c) show that, electrons are localized on Se-atom sites, and the Ge-Se bond strength along b direction is weaker than that along a direction. Therefore, when applying tensile strains along b direction, the overlap integral will not fluctuate greatly due to the weak covalent bonds along b direction, which may subsequently lead to the robust band gap insensitive to the tensile strains along b direction as shown in Fig. 5(d).

D. Transport properties of black phosphorene, monolayer $\alpha-$MX and $\beta-$GeSe

To investigate the transport properties of $\alpha-$ and $\beta-$GeSe, we systematically calculate carrier mobilities of black phosphorene, monolayer $\alpha-$MX ($\alpha-$GeS, $\alpha-$GeSe, $\alpha-$SnS and $\alpha-$SnSe) and $\beta-$GeSe. According to the deformation theory, *i.e.* Eq. (5), three parameters, namely carrier effective mass m^*, the deformation potential E_l and the elastic modulus C^{2D} in the propagation direction determine the behaviors of carrier mobility of semiconductors[43, 58]. Although the PBE calculations always underestimate the band gap, the curvatures of valence and conduction bands calculated by PBE method are generally correct enough and the calculated carrier mobilities are subsequently in good agreement with experiments for numerous 2D materials[41–43, 58, 59]. We calculate the effective masses of holes (m_h^*) and electrons (m_e^*) along a and b directions by fitting parabolic func-

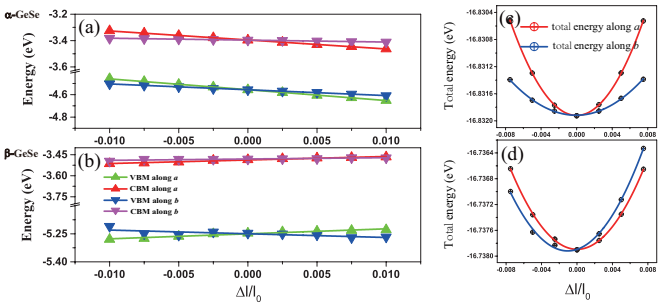

FIG. 7. Dependence of band edges with respect to vacuum as a function of applied uniaxial strains along a and b directions for monoalayer (a) $\alpha-$ and (b) $\beta-$GeSe, respectively. (c) and (d) shows the relationship between total energy and strain along a and b directions for $\alpha-$ and $\beta-$GeSe, respectively.

tions to the band curve close to the VBM and CBM, respectively, as shown in Table. II.

For black phosphorene, it is remarkable that along the a direction (band structure along Γ-X direction in Supplemental Material[47]), the valence of band is nearly flat close to the Γ point (VBM), with the effective hole mass of 11.16 m_0, 9 times larger than the effective electron mass (1.24 m_0). And along b direction (Γ-Y direction in band structure), the effective carrier masses are 0.14 m_0 (hole) and 0.15 m_0 (electron) respectively, mainly due to the more dispersive s and p characters of VBM and CBM as shown in the band structure along the Γ-Y direction (see Supplemental Material[47]).

As mentioned above, monolayer $\alpha-$MX can be regarded as the "phosphorene analogues" produced by the so-called "atomic transmutation" method, the band structures of the four monolayer $\alpha-$MXs, *i.e.* $\alpha-$GeS, $\alpha-$GeSe, $\alpha-$SnS and $\alpha-$SnSe, indeed show similar patterns, which are shown in Fig. 2(a) and Supplemental Material[47]. All the four monolayer $\alpha-$MXs possess CBM along the $\Gamma - X$ and VBM along the $\Gamma - Y$ directions. According to the d^{-2} principle[53], the orbital overlapping integral V also determines the bandwidth of a specific band, and generally a band with a larger bandwidth has a larger band curvature at the CBM/VBM points, which thus leads to a smaller effective electron/hole masses for covalent solids. As shown in the Table. S1, the bond lengths $d_{1/2}$ for all the monolayer $\alpha-$MXs have the tendency of $d_{GeS} < d_{GeSe} < d_{SnS} < d_{SnSe}$, therefore, the orbital overlapping V should be $V_{GeS} > V_{GeSe} > V_{SnS} > V_{SnSe}$, since the conduction and valence bands of all the monolayer $\alpha-$MXs are formed by $M - p$ and $X - p$ orbitals respectively. Subsequently, the effective masses for all the monolayer $\alpha-$MXs can be ordered by $m^*_{GeS} > m^*_{GeSe} > m^*_{SnS} > m^*_{SnSe}$, due to the opposite tendency of the bandwidths for these four monolayer $\alpha-$MXs. The relation of the effective masses for all the monolayer $\alpha-$MXs is shown and confirmed in Table. II as well.

By linearly fitting the band energy (CBM and VBM positions) shift with respect to the vacuum level under strain $\varepsilon(\Delta l/l_0)$ along a and b directions, the DP constant E_l for both electrons and holes can be calculated. As shown in Fig. 7 (a) and (b), the responses of CBM and VBM for $\alpha/\beta-$GeSe to the applied strain appear to be anisotropic as well. The response for black phosphorene, $\alpha-$GeS, $\alpha-$SnS and $\alpha-$SnSe are shown in Supplemental Material[47]. The obtained DP constants E_l are listed in Table. II.

The elastic constant C^{2D} can be calculated from the relation between the total energy and lattice dilations. Such relations for all the 2D materials under investigation here are shown in Fig. 7 (c-d) and Supplemental Material[47]. The calculated elastic constants are listed in Table. II.

Based on the obtained m^*_e, E_l and C^{2D}, the carrier mobilities of black phosphorene, monolayer $\alpha-$MX ($\alpha-$GeS, $\alpha-$GeSe, $\alpha-$SnS and $\alpha-$SnSe) and $\beta-$GeSe at room temperature (T=300 K) are calculated and listed in Table. II. For black phosphorene, it has a large hole carrier mobility of $1.13\times10^4 cm^2/V\cdot s$ along the a direction, even with large hole effective mass of 11.16 m_0, but with large elastic modulus of 102.59 N/m which is expected from the hybridized covalent sp^3 bonds and extremely small band edge deformation potential constant of 0.12 eV, which can be understood by considering the band edge wave function that the distribution of electron state can have a significant impact on the lattice deformation[21]. Table. II also shows the transport properties of monolayer $\alpha-$MX, which show strongly anisotropic transport properties and high carrier mobilities along a or b directions.

The predicted carrier mobilities for both $\alpha-$ and $\beta-$GeSe are anisotropic along the a and b directions. Both $\alpha-$ and $\beta-$GeSe show high electron mobilities along the b direction (μ_b), *i.e.* $4.71\times10^3 cm^2/V\cdot s$ for monolayer $\alpha-$GeSe and $2.93\times10^4 cm^2/V\cdot s$ for monolayer $\beta-$GeSe, respectively. The calculated value of μ_b for $\beta-$GeSe is comparable to that of black phosphorene ($1.13\times10^4 cm^2/V\cdot s$), which suggests that monolayer $\beta-$GeSe is also a promising candicate material for future electronic and optoelectronic applications, considering the high electron mobilities and stability in ordinary environment[27].

E. Optical properties of monolayer $\alpha-$ and $\beta-$GeSe

Fig. 8 presents the in-plane optical absorption spectra $\alpha(\omega)$ and reflectivity $R(\omega)$ of monolayer $\alpha-$ and $\beta-$GeSe for the incident light with the polarization of the electric field $\mathbf{E}$ along the a ($\mathbf{E}//a$) and b ($\mathbf{E}//b$) directions respectively. In 2D materials, compared to the band gap calculated by quasi-particle GW method which considers the excitonic effects, the optical band gap obtained by HSE06 is usually close to the real optical band gap due to the underestimation of band gap by neglecting excitonic effects[21]. Thus, we only perform HSE06 cal-

TABLE II. Calculated band gap E_g, effective mass m^* (with m_0^* being the static electron mass), deformation potential constant E_l, 2D elastic modulus C and carrier mobility μ along the $\Gamma - X$ and $\Gamma - Y$ directions respectively. The electron and hole carrier mobilities μ are calculated by using Eq. (5) at T=300 K.

Phase	$E_g(HSE06)$ $[eV]$	carrier type	m_a^* $[m_0]$	m_b^*	E_{l-a} $[eV]$	E_{l-b}	C_a $[N/m]$	C_b	μ_a $[cm^2/V\cdot s]$	μ_b $[cm^2/V\cdot s]$
black phosphorene	1.49	hole	11.16	0.14	0.12	2.79	102.59	23.60	1.13×10^4	3.66×10^2
		electron	1.24	0.15	5.28	1.58	102.59	23.60	1.46×10^2	3.08×10^3
$\alpha-$GeS	2.75	hole	0.87	0.25	4.57	6.45	42.36	12.89	1.06×10^2	5.70×10^1
		electron	0.46	0.23	3.24	0.47	42.36	12.89	5.73×10^2	1.69×10^4
$\alpha-$GeSe	1.61	hole	0.33	0.16	9.67	5.20	37.00	14.00	1.10×10^2	3.10×10^2
		electron	0.27	0.15	6.83	1.45	37.00	14.00	3.07×10^2	4.71×10^3
$\alpha-$SnS	1.50	hole	0.30	0.22	5.91	4.03	38.43	17.08	3.08×10^2	3.92×10^2
		electron	0.21	0.19	3.16	2.72	38.43	17.08	1.93×10^3	1.27×10^3
$\alpha-$SnSe	0.98	hole	0.16	0.14	8.40	4.74	41.65	21.32	5.40×10^2	9.42×10^2
		electron	0.13	0.14	2.53	1.84	41.65	21.32	7.64×10^3	7.31×10^3
$\beta-$GeSe	2.47	hole	1.09	0.84	2.68	1.99	42.00	41.00	1.19×10^2	2.71×10^2
		electron	1.45	0.09	2.52	0.96	42.00	41.00	2.71×10^2	2.93×10^4

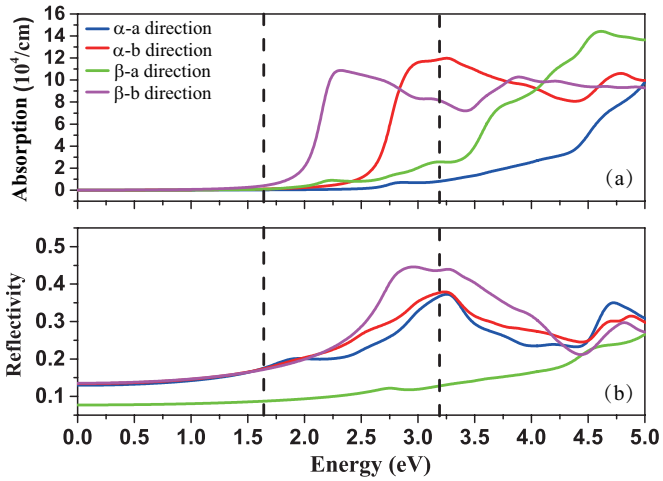

FIG. 8. HSE06 calculations of (a) optical absorption spectra and (b) reflectivity of monolayer $\alpha-$ and $\beta-$GeSe for incident light with the polarization along the a and b directions.

culations of optical properties here. And it deserves further investigations on excitonic effects on electronic and optical properties of monolayer $\alpha-$ and $\beta-$GeSe. The corresponding imaginary part of the dielectric function are shown in Supplemental Material[47].

The absorption coefficient is defined as the decay of light intensity spreading in a unit length, *i.e.* Eq. (3). For monolayer $\alpha-$ and $\beta-$GeSe, the absorption coefficient shows an obvious anisotropy along different directions, and both materials exhibit obvious optical absorption with the frequency covering some part of the visible spectrum. The frequency region for high absorption along the b direction of $\beta-$GeSe is larger than that along the a direction shown in Fig. 8 (a), and is even larger than those of $\alpha-$GeSe irrespective of polarization directions. Such a significant anisotropic optical property can be used to identify the monolayer $\beta-$GeSe in experiments.

Fig. 8 (b) shows the reflectivity $R(\omega)$ for both monolayer $\alpha-$ and $\beta-$GeSe. The relatively less anisotropic property of $\alpha-$GeSe and anisotropic for $\beta-$GeSe are observed in the reflectivity curves as shown in Fig. 8 (b). For $\beta-$GeSe, $R(\omega)$ along the b direction in the visible region is higher than that of $\alpha-$GeSe along both a and b directions, which thus means that monolayer $\beta-$GeSe is polarizationally non-transparent material.

IV. CONCLUSION

In summary, we have performed first-principles calculations on the structure, electronic, transport and optical properties of monolayer $\alpha-$ and $\beta-$GeSe. $\alpha-$GeSe is a puckered structure similar to that of black phosphorene with Ge and Se atoms substituted for P atoms alternately, while $\beta-$GeSe consists of six-rings with the vertices arranged in an uncommon boat conformation. They all have strongly anisotropic properties. For monolayer $\alpha-$GeSe, the direct-semiconducting characteristic is robust for small compression and moderate stretching along b direction (from ε_x=-1% to ε_x=9%), and an extremely high electron mobility of $2.93\times10^4 cm^2/V\cdot s$ for $\beta-$GeSe is observed along the armchair direction. Furthermore, the band gaps of monolayer $\beta-$GeSe keep nearly unchanged under tensile strain from 0% to 10%. The calculated optical properties of monolayer $\alpha-$ and $\beta-$GeSe shows anisotropic behaviors and large absorption in some part of visible spectrum. Due to the ultrahigh electron mobilities and the abnormal behavior of robust band gap disregarding the applied tensile strains, monolayer $\beta-$GeSe is promising in the future electronic and optoelectronic applications.

ACKNOWLEDGEMENT

This work is supported by the National Natural Science Foundation of China under Grants No. 11374063 and 11404348, and the National Basic Research Program of China (973 Program) under Grants No. 2013CBA01505. Work at Ames Laboratory is partially supported by the U.S.Department of Energy, Office of Basic Energy Science, Division of Materials Science and Engineering (Ames Laboratory is operated for the U.S. Department of Energy by Iowa State University under Contract No. DE-AC02-07CH11358). The European Research Council under ERC Advanced Grant No. 320081 (PHOTOMETA) supports work at FORTH.

REFERENCE

[1] K. S. Novoselov, A. K. Geim, S. V. Morozov, D. Jiang, Y. Zhang, S. V. Dubonos, I. V. Grigorieva, and A. A. Firsov. Electric field effect in atomically thin carbon films. Science, **306**, 666(2004).

[2] K. S. Novoselov, A. K. Geim, S. V. Morozov, D. Jiang, Katsnelson M. I., I. V. Grigorieva, and A. A. Dubonos, S. V.and Firsov. Two-dimensional gas of massless dirac fermions in graphene. Nature, **438**, 197(2005).

[3] Y. B. Zhang, Y. W. Tan, H. L. Stormer and P. Kim. Experimental observation of the quantum hall effect and berry's phase in graphene. Nature, **438**, 201(2005).

[4] A. A. Balandin. Thermal properties of graphene and nanostructured carbon materials. Nat. Mater., **10**, 569(2011).

[5] A. A. Balandin, S. Ghosh, W. Z. Bao, I. Calizo, D. Teweldebrhan, F. Miao, and C. N. Lau. Superior thermal conductivity of single-layer graphene. Nano Lett., **8**, 902(2008).

[6] F. Schedin, A. K. Geim, S. V. Morozov, E. W. Hill, P. Blake, M. I. Katsnelson, and K. S. Novoselov. Detection of individual gas molecules adsorbed on graphene. Nat. Mater., **6**, 652(2007).

[7] K. Kaasbjerg, K. S. Thygesen, and K. W. Jacobsen. Phonon-limited mobility in n-type single-layer mos_2 from first principles. Phys. Rev. B, **85**, 115317(2012).

[8] H. J. Conley, B. Wang, J. I. Ziegler, Jr. Richard F. Haglund, S. T. Pantelides, and K. I. Bolotin. Bandgap engineering of strained monolayer and bilayer mos_2. Nano Lett., **13**, 3626(2013).

[9] W. S. Yun, S. W. Han, S. C. Hong, I. G. Kim, and J. D. Lee. Thickness and strain effects on electronic structures of transition metal dichalcogenides: 2h-mX_2 semiconductors (m = mo, w; x = s, se, te). Phys. Rev. B, **85**, 033305,(2012).

[10] A. Kumar and P. K. Ahluwalia. Electronic structure of transition metal dichalcogenides monolayers 1h-mx2 (m = mo, w; x = s, se, te) from ab-initio theory: new direct band gap semiconductors. Eur. Phy. J. B, **85**, 186(2012).

[11] F. F. Zhu, W. J. Chen, Y. Xu, C. L. Gao, D. D. Guan, C. H. Liu, D. Qian, S. C. Zhang, and J. F. Jia. Epitaxial growth of two-dimensional stanene. Nat Mater., **14**, 1020(2015).

[12] S. Balendhran, S. Walia, H. Nili, S. Sriram, and M. Bhaskaran. Elemental analogues of graphene: Silicene, germanene, stanene, and phosphorene. Small, **11**, 640(2015).

[13] S. H Zhang, J. Zhou, Q. Wang, X. S. Chen, Y. Kawazoe, and P. Jena. Penta-graphene: A new carbon allotrope. Proc. Natl. Acad. Sci., **112**, 2372(2015).

[14] Y.F. Xu, Z. Y. Ning, H. Zhang, G. Ni, H. Z. Shao, B. Peng, X. C. Zhang, X. Y. He, Y. Y. Zhu, and H. Y. Zhu. Anisotropic ultrahigh hole mobility in twodimensional penta-sic2 by strain-engineering: electronic structure and chemical bonding analysis. RSC Adv., **7**, 45705(2017).

[15] J. S. Qiao, X. H. Kong, Z. X. Hu, F. Yang, and W. Ji. High-mobility transport anisotropy and linear dichroism in few-layer black phosphorus. Nat. Commun., **5**, 1(2014).

[16] T. Hong, B. Chamlagain, W. Z. Lin, H. J. Chuang, M. Pan, Z. X. Zhou, and Y. Q. Xu. Polarized photocurrent response in black phosphorus field-effect transistors. Nanoscale, **6**, 8978(2014).

[17] H. Liu, A. T. Neal, Z. Zhu, Z. Luo, X. F. Xu, D. Tomanek, and P. D. Ye. Phosphorene: An unexplored 2d semiconductor with a high hole mobility. Acs. Nano., **8**, 4033(2014).

[18] J. Liu, G. M. Choi, and D. G. Cahill. Measurement of the anisotropic thermal conductivity of molybdenum disulfide by the time-resolved magneto-optic kerr effect. J. Appl. Phys., **116**, 233107(2014).

[19] V. Eswaraiah, Q. S. Zeng, Y. Long, and Z. Liu. Black phosphorus nanosheets: Synthesis, characterization and applications. small, **12**, 3480(2016).

[20] L. C. Gomes and A. Carvalho. Phosphorene analogues: Isoelectronic two-dimensional group-iv monochalcogenides with orthorhombic structure. Phys. Rev. B, **92**, 085406(2015).

[21] J. H. Yang, Y. Y. Zhang, W. J. Yin, X. G. Gong, B. I. Yakobson, and S. H. Wei. Two-dimensional sis layers with promising electronic and optoelectronic properties: theoretical prediction. Nano lett., **16**, 1110(2016).

[22] Y.G. Zhou. Mx (m = ge, sn; x = s, se) sheets: theoretical prediction of new promising electrode materials for li ion batteries. J. Mater. Chem., **4**, 10906(2016).

[23] H. Wang and X. F. Qian. Two-dimensional multiferroics in monolayer group iv monochalcogenides. 2D Mater., **4**, 015042(2017).

[24] R. X Fei, W. B. Li, J. Li, and L. Yang. Giant piezoelectricity of monolayer group iv monochalcogenides: Snse, sns, gese, and ges. Appl. Phys. Lett., **107**, 173104(2015).

[25] A. Shafique and Y. H. Shin. Thermoelectric and phonon transport properties of two-dimensional iv-vi compounds. Sci. Rep., **7**, 506(2017).

[26] L. D. Zhao, S.H. Lo, Y. S. Zhang, H. Sun, G. J. Tan, C. Uher, C. Wolverton, V. P. Dravid, and M. G.

Kanatzidis. Ultralow thermal conductivity and high thermoelectric figure of merit in snse crystals. Nature, **508**, 373(2014).

[27] F. O. von Rohr, H. W. Ji, F. A. Cevallos, T. Gao, N. P. Ong, and R. J. Cava. High-pressure synthesis and characterization of β-gese-a semiconductor with six-rings in an uncommon boat conformation. J. Am. Chem. Soc., **139**, 2771(2017).

[28] H. Wiedemeier, von Schnering, and H. Georg. Refinement of the structures of ges, gese, sns and snse. Zeitschrift für Kristallographie-Crystalline Materials, **148**, 295(1978).

[29] G. Kresse and J. Furthmüller. Efficient iterative schemes for *ab initio* total-energy calculations using a plane-wave basis set. Phys. Rev. B, **54**, 11169(1996).

[30] J. Heyd, G. E. Scuseria, and M. Ernzerhof. Hybrid functionals based on a screened coulomb potential. J. Chem. Phys., **118**, 8207(2003).

[31] J. Heyd, G. E. Scuseria, and M. Ernzerhof. Erratum: ybrid functionals based on a screened coulomb potential?[j. chem. phys. 118, 8207 (2003)]. J. Chem. Phys., **124**, 219906(2006).

[32] J. P. Perdew, K. Burke, and M. Ernzerhof. Generalized gradient approximation made simple. Phys. Rev. Lett., **77**, 3865(1996).

[33] S. Grimme. Semiempirical gga-type density functional constructed with a long-range dispersion correction. J. Comput. Chem., **27**, 1787(2006).

[34] M. Gajdoš, K. Hummer, G. Kresse, J. Furthmüller, and F. Bechstedt. Linear optical properties in the projector-augmented wave methodology. Phys. Rev. B, **73**, 045112(2006).

[35] MS. Dresselhaus. Solid State Physics Part II Optical Properties of Solids. Citeseer, 1999.

[36] S. Saha, T. P. Sinha, and A. Mookerjee. Electronic structure, chemical bonding, and optical properties of paraelectric batio$_3$. Phys. Rev. B, **62**, 8828(2000).

[37] B. C. Luo, X. H. Wang, E. Tian, G. W. Li, and L. T. Li. Electronic structure, optical and dielectric properties of batio$_3$/catio$_3$/srtio$_3$ ferroelectric superlattices from first-principles calculations. J. Mater. Chem. C, **3**, 8625(2015).

[38] Y. F. Xu, B. Peng, H. Zhang, H. Z. Shao, R. J. Zhang, and H. Y. Zhu. First-principle calculations of optical properties of monolayer arsenene and antimonene allotropes. *Ann. Phys. (Berlin)*, 1600152(2017).

[39] J. Bardeen and W. Shockley. Deformation potentials and mobilities in non-polar crystals. Phys. Rev., **80**, 72(1950).

[40] Y. Nakamura, T. Q. Zhao, J. Y. Xi, W. Shi, D. Wang, and Z. G. Shuai. Intrinsic charge transport in stanene: Roles of bucklings and electron-phonon couplings. arXiv preprint arXiv:1705.01816, 2017.

[41] Y. Cai, G. Zhang, and Y.W Zhang. Polarity-reversed robust carrier mobility in monolayer mos$_2$ nanoribbons. J. Am. Chem. Soc., **136**, 6269(2014).

[42] M. Q. Long, L. Tang, D. Wang, Y. L. Li, and Z. G. Shuai. Electronic structure and carrier mobility in graphdiyne sheet and nanoribbons: Theoretical predictions. ACS Nano., **5**, 2593(2011).

[43] J. M. Chen, J. Y. Xi, D. Wang, and Z. G. Shuai. Carrier mobility in graphyne should be even larger than that in graphene: A theoretical prediction. J. Phys. Chem. Lett., **4**, 1443(2013).

[44] Y. L. Wang and Y. Ding. Electronic structure and carrier mobilities of arsenene and antimonene nanoribbons:a first-principle study. Nanoscale Res. Lett., **10**, 254(2015).

[45] F. Li, X. H. Liu, Y. Wang, and Y. F. Li. Germanium monosulfide monolayer: a novel two-dimensional semiconductor with a high carrier mobility. J. Mater. Chem. C, **4**, 2155(2016).

[46] R. X. Fei and L. Yang. Strain-engineering the anisotropic electrical conductance of few-layer black phosphorus. Nano Lett., **14**, 2884(2014).

[47] See supplemental material at [url will be inserted by publisher] for details of data analysis.

[48] Y. D. Hu, S. L. Zhang, S. F. Sun, M. Q. Xie, B. Cai, and H. B. Zeng. Gese monolayer semiconductor with tunable direct band gap and small carrier effective mass. Appl. Phys. Lett., **107**, 122107(2015).

[49] M. H. Wu and X. C. Zeng. Intrinsic ferroelasticity and/or multiferroicity in two-dimensional phosphorene and phosphorene analogues. Nano lett., **16**, 3236(2016).

[50] A. K. Singh and R. G. Hennig. Computational prediction of two-dimensional group-iv mono-chalcogenides. Appl. Phys. Lett., **105**, 042103(2014).

[51] C. Si, Z. M. Sun, and F. Liu. Strain engineering of graphene: a review. Nanoscale, **8**,3207–3217(2016).

[52] R. Qin, C. H. Wang, W. J. Zhu, and Y. L. Zhang. First-principles calculations of mechanical and electronic properties of silicene under strain. AIP Advances, **2**, 022159(2012).

[53] Y. K. Sun, S. E. Thompson, and T. Nishida. *Strain Effect in Semiconductors*. Springer, 2010.

[54] A. D. Becke and K. E. Edgecombe. A simple measure of electron localization in atomic and molecular systems. J. Chem. Phys., **92**, 5397(1990).

[55] A. Savin, O. Jepsen, J. Flad, O. K. Andersen, H. Preuss, and H. G. von Schnering. Electron localization in solid-state structures of the elements: the diamond structure. Angew. Chem. Int. Ed. Engl., **31**, 187(1992).

[56] C. Gatti. Chemical bonding in crystals: new directions. Zeitschrift für Kristallographie-Crystalline Materials, **220**, 399(2005).

[57] K. Chen and S. Kamran. Bonding characteristics of tic and tin. Modeling and Numerical Simulation of Material Science, **3**, 7(2013).

[58] J. Y. Xi, M. Q. Long, L. Tang, D. Wang, and Z. G. Shuai. First-principles prediction of charge mobility in carbon and organic nanomaterials. Nanoscale, **4**, 4348(2012).

[59] J. Dai and X. C. Zeng. Titanium trisulfide monolayer: Theoretical prediction of a new direct-gap semiconductor with high and anisotropic carrier mobility. Angew. Chem., **127**, 7682(2015).